REVISION 1

Qingsongite, natural cubic boron nitride: The first boron mineral from the Earth's mantle

Larissa F. Dobrzhinetskaya[1]*, Richard Wirth[2], Jingsui Yang[3], Harry W. Green[1], Ian D. Hutcheon[4], Peter K. Weber[4] and Edward S. Grew[5]

[1]Department of Earth Sciences, University of California at Riverside, 900 University Avenue, Riverside, CA 92521, USA,

[2]Helmholtz Centre Potsdam, GFZ German Research Centre for Geosciences, Section 3.3, Chemistry and Physics of Earth Materials, Telegrafenberg, C 120, D-14473 Potsdam, Germany

[3]Key Laboratory for Continental Dynamics, Institute of Geology, Chinese Academy of Geological Sciences, 26 Baiwanzhuang Road, Beijing, 100037, PRC

[4]Glenn T. Seaborg Institute, Lawrence Livermore National Laboratory, 7000 East Avenue, Livermore, CA 94550, USA

[5]School of Earth and Climate Sciences, 5790 Bryand Global Sciences Center, University of Maine, Orono, ME 04469-5790, USA

*E-mail: larissa@ucr.edu

To be submitted to American Mineralogist

Abstract

Qingsongite (IMA 2013-30) is the natural analogue of cubic boron nitride (c-BN), which is widely used as an abrasive under the name "Borazon". The mineral is named for Qingsong Fang (1939—2010), who found the first diamond in the Luobusa chromite. Qingsongite occurs in a rock fragment less than 1 mm across extracted from chromite in deposit #31, Luobusa ophiolite, Yarlung Zangbu suture, southern Tibet at 29°13.86N and 92°11.41E. Five electron microprobe analyses gave B 48.54 ±0.65 wt% (range = 47.90 – 49.2 wt%); N 51.46 ±0.65 wt% (range 52.10

- 50.8 wt%), corresponding to $B_{1.113}N_{0.887}$ and $B_{1.087}$ $N_{0.913,}$ for maximum and minimum B contents, respectively (based on 2 atoms per formula unit); no other elements that could substitute for B or N were detected. Crystallographic data on qingsongite obtained using fast Fourier transforms gave cubic symmetry, a = 3.61 ± 0.045 Å. The density calculated for the mean composition $B_{1.100}N_{0.900}$ is 3.46 g cm^{-3}, i.e., qingsongite is nearly identical to synthetic c-BN. The synthetic analogue has the sphalerite structure, space group *F*-43*m.* Mohs hardness of the synthetic analogue is between 9 and 10; its cleavage is {011}. Qingsongite forms isolated anhedral single crystals up to 1 μm in size in the marginal zone of the fragment; this zone consists of ~45 modal % coesite, ~ 15% kyanite and ~ 40% amorphous material. Qingsongite is enclosed in kyanite, coesite or in osbornite; other associated phases include native Fe; TiO_2 II, a high-pressure polymorph of rutile with the αPbO_2 structure; boron carbide of unknown stoichiometry; and amorphous carbon. Coesite forms prisms several tens of μm long, but is polycrystalline, and thus interpreted to be pseudomorphic after stishovite. Associated minerals constrain the estimated pressure to 10-15 GPa assuming temperature was about 1300 °C. Our proposed scenario for formation of qingsongite begins with a pelitic rock fragment that was subducted to mid-mantle depths where crustal B originally present in mica or clay combined with mantle N ($\delta^{15}N$ = 10.4 ± 3 ‰ in osbornite) and subsequently exhumed by entrainment in chromitite.

Introduction

Boron is quintessentially an element of the Earth's upper continental crust, as the crust is markedly enriched in B (17 ppm B, Rudnick and Gao 2005) relative to primitive mantle (0.26 ppm B, Palme and O'Neill 2005) and CI chondrite (0.775 ppm B, Lodders 2010). Leeman and Sisson (2002) concluded that the transfer of boron from the mantle to the crust is "essentially unidirectional", that is, little, if any, boron is returned to the mantle, even in deeply subducted crust, and thus the concentration of B in the upper continental crust is expected to increase with the passage of time. A corollary of this concentration is that none of the 262 valid minerals in the IMA list known to contain essential B (http://rruff.info/ima/) has been reported either in mantle rocks or in meteorites; all are found in rocks of clearly crustal origin and many are water soluble compounds found at or near the Earth's surface.

A possible exception to this distribution is cubic boron nitride, c-BN, which Dobrzhinetskaya et al. (2009) reported from a kyanite-coesite-bearing silicate assemblage rimming a core of Fe-Ti alloy in a rock fragment less than 1 mm across extracted from chromite in deposit #31, Luobusa ophiolite, Yarlung Zangbu suture, southern Tibet at 29°13.86N and 92°11.41E (Fig. 1), and now approved as the new mineral qingsongite (IMA 2013-30, Dobrzhinetskaya et al. 2013). Cubic-BN (c-BN) was synthesized for the first time in 1957 by General Electric Co from hexagonal boron nitride (h-BN) in the presence of metal solvent catalysts (Wentorf, 1957, 1961). Synthetic c-BN is isostructural with sphalerite (Solozhenko et al. 1990; Eichhorn et al. 1991), which in the industrial literature is referred to as "zincblende"; i.e., c-BN has cubic closest-packing and is a homeotype of diamond. Synthetic c-BN is second only to diamond in hardness (Gardinier 1988), and thus has found wide use as an abrasive material under the trade name "Borazon;" it also has potential applications in electronics and ceramics (Wentorf 1957, 1961; Vel et al. 1991; Haubner et al. 2002; Horwath-Bordon et al., 2006). Earlier it was thought that synthesis of stable c-BN can be performed only at high pressures and high temperatures (e.g., > 40 GPa, >1200 °C, Corrigan and Bundy 1975), but further experimental and theoretical studies reported successful synthesis at relatively low pressures and temperatures, e.g., at 1.5-2.0 GPa and 500-700 °C in supercritical hydrazine, N_2H_4, with Li_3N as an additive (Demazeau et al. 1995). Nonetheless, because catalysis, nucleation and solvents play major roles in c-BN synthesis (e.g., Wang et al. 2004), the stability of c-BN relative to other BN polymorphs such as h-BN, rhombohedral BN (r-BN), and wurtzite-structured BN (w-BN) polymorphs are still controversial.

In considering the origin of qingsongite, leading questions are not only the conditions of formation, which can be constrained by stability field of its host mineral (coesite pseudomorphous after stishovite), but also the source of boron and nitrogen for a mineral formed at a depth estimated to be at least 300 km (Dobrzhinetskaya et al., 2009). The only B concentrations exceeding 1 ppm in minerals from mantle depths are reported in type IIb blue diamonds (1-8 ppm B, N < 5-10 ppm, Gaillou et al. 2012), and it is thought that B in diamonds could have been sourced from the crust. In general, nitrogen impurities are widespread in kimberlitic-lamproitic diamond and abundances can range 3 orders of magnitude depending on the source of the diamond (e.g., a few ppm to over 1000 ppm, Palot et al. 2012); diamonds from

ultrahigh-pressure metamorphic terrains contain up to 11,000 ppm N (Dobrzhinetskaya et al. 2010).

Mineral name and type material

The c-BN mineral and its name qingsongite have been approved by the Commission on New Minerals and Mineral Names (CNMMN) of the International Mineralogical Association (IMA 2013-30) (Dobrzhinetskaya et al., 2013); it had been included in the list of Valid Unnamed Minerals (Smith and Nickel 2007) as UM2009-32-N:B – BN (boron nitride). The mineral was named in honor of Qingsong Fang (1939－2010), Professor at the Institute of Geology, Chinese Academy of Geological Sciences, who found the first diamond in the Luobusa chromite in the late 1970s, and contributed to the discovery of four new species: yarlongite, zangboite, qusongite and luobusaite in the Luobusa ophiolite. Type material is deposited in the collections of the Geological Museum of China, 15 Yangrouhutong, Xisi, West District, Beijing 100034, PRC, catalogue number M 11843.

Appearance, physical and optical properties

Qingsongite forms isolated anhedral single crystals from 100 nm up to 1 μm in size. Because qingsongite is a nanomineral that occurs in quantities far too small for characterization of the physical and optical properties readily measured in larger samples, we have cited measurements on the synthetic analogue. Mohs hardness of the synthetic analogue is between 9 and 10; its cleavage is {011} (Gardinier, 1988). The calculated density is 3.46 g cm^{-3} assuming the average composition $B_{1.100}N_{0.900}$ and cell parameter of 3.61 Å; densities reported for synthetic analogues are 3.488(3) g cm^{-3} (Soma *et al*. 1974) and 3.487 g cm^{-3} (Eichhorn *et al*. 1991). Synthetic c-BN is colorless, but impurities can render it yellow, orange or black (Haubner et al. 2002; Wang et al. 2003). Refractive index at 589.3 nm (sodium light) is estimated to be 2.117 in the synthetic analogue (Gielisse et al., 1967).

Chemical composition

Energy dispersive (ED) X-ray analysis was used to determine chemical composition (Fig. 2 a, b). Spectra were acquired with a JEOL JXA-8900 Super Probe and with a Transmission Electron Microscope (Technai-F20 XTWIN) operating at 200 kV with a field emission electron source in

the scanning transmission mode (STEM) by using the TIA software package for data evaluation. TEM foils were prepared with a FEI Focus Ion beam (FIB) device. Significant mass loss during analysis with the TEM was avoided by scanning the beam in a preselected window (according to the size of the measured volume). Spot size was 1 nm, and acquisition time was 60 s.

The EDX spectra show only boron (B) and nitrogen (N); no other element that could substitute for B or N, e.g., C, was detected (Fig 2 b). The Si, O, Ti, Cu and Ga X-ray photon intensities in the spectra originated from the host coesite, osbornite, Cu-grid and from gallium implanted during FIB milling, respectively. No carbon coating was applied to the FIB-foils, and therefore we exclude the possibility that boron was misidentified as carbon, because the peaks are resolved in EDX spectra (C-K_α = 0.277 keV and B-K_α = 0.183 keV).

The presence of both boron and nitrogen and the absence of carbon in each measured crystal of qingsongite were additionally verified with Electron Energy Loss Spectroscopy (EELS), which gave a 1:1 atomic ratio (Fig. 3 a,b). Element mapping of the boxed area shown on Fig. 2a clearly indicates that the areas for B, N and Ti corresponding to c-BN and TiN (Fig. 4 a-d) do not overlap with the area of silicon and oxygen (Fig. 4 e,f) corresponding to coesite.

The chemical composition of qingsongite was also measured with a JEOL JXA-8900 Super Probe electron microprobe in the wavelength dispersive spectroscopic (WDS) mode at 15 kV accelerating potential and 20 nA probe current, a 1 μm beam size and a counting period of 10 s. Quantitative analyses were carried out without standards using the $\phi(\rho Z)$ method for correction (JEOL Ltd, 1993-handouts); the 1 sigma error of measurements is 2%. Five analyses gave B 48.54 ±0.65 wt% (range = 47.90 – 49.2 wt%); N 51.46 ±0.65 wt% (range 52.10 - 50.8 wt%), whereas stoichiometric c-BN has the composition of 43.6 wt% B and 56.4 wt% N. Formulas calculated from the maximum B and minimum N, and minimum B and maximum N contents gave $B_{1.113}N_{0.887}$ and $B_{1.087}$ $N_{0.913,}$ respectively, suggesting excess of boron not detected in the EELS. Excess boron has also been reported in synthetic c-BN, i.e., analysis of the first synthesis gave $B_{1.035}N_{0.965}$ (Wentorf 1957). Black color in synthetic c-BN has been attributed to excess B (Wentorf 1961; Haubner et al. 2002; Bogdanov 2008). Bogdanov's (2008) detailed study showed that extra B atoms can be incorporated in c-BN, resulting not only in an increase in the lattice

parameter *a*, as had been reported by another investigator, but also in a distortion of the structure. Thus, excess B in natural c-BN is plausible, but more precise and better calibrated chemical analysis would be needed to determine whether non-stoichiometry is real and not merely an artifact of the analytical method.

Crystallography

Crystallographic data on qingsongite were obtained with the Technai-F20 XTWIN instrument operating at 200 kV using a field emission electron source. Fast Fourier transforms (FFT) were calculated from high-resolution lattice fringe images by measuring the lengths of the different vectors displayed in the diffraction patterns (Fig. 5). The FFT were calibrated with graphite that is present in the same foil and an external albite standard: the standard deviation was 0.06 Å for 10 measurements in albite. In addition, we used Pt that was deposited on the top of the foil prior to FIB sputtering as internal standards for calibrating the qingsongite lattice parameter (Table 1). Our calculations gave a lattice parameter of 3.61 Å for qingsongite. We have calculated that the average of absolute values of the differences between measured and literature values for d_{hkl} is 0.045 Å, and that the standard deviation is 0.046 Å (Table 1).Given this standard deviation, our cell parameter is consistent with cell parameters reported for synthetic c-BN, which range from 3.6150 to 3.6160 Å with uncertainties between 0.001 and 0.0001 Å (Wentorf 1957; Soma et al. 1974; Will et al. 1986; Eichhorn et al. 1991; Solozhenko et al. 1990).

The correct indexing of the diffraction patterns as c-BN was re-checked by comparing the observed angles between corresponding vectors in the diffraction patterns with the angles between adjacent planes from literature data. Additionally, we calculated the angles between adjacent planes in the diffraction pattern with zone axis 00-1 and compared them with the observed angles (Table 2). All of the angles are within the measurement error of < 1°. The measurement of the angles between adjacent planes and the agreement between calculated and observed angles confirms the identification of qingsongite as c-BN. By analogy with the synthetic compound, qingsongite has space group $F\text{-}43m$, $Z = 4$.

Powder X-ray diffraction data (Table 3) are taken from Soma *et al.* (1974) for the synthetic analogue with $a = 3.6157$ (10) Å.

Occurrence and associated minerals

The qingsongite-bearing rock fragment comprises three zones: (1) a core of Fe-Ti alloy about 500 μm across is mantled by (2) an inner zone 10-90 μm thick of native Ti, which in turn is partially mantled by (3) an outer zone of aluminosilicate minerals 30-60 μm thick (Yang et al. 2007; Dobrzhinetskaya et al. 2009). A very narrow zone (<1 μm) of Si-Al alloy (Si 78, Al 20, Ti 2, in at. %) borders the native Ti adjacent to the aluminosilicate zone, which consists of ~45 modal % coesite, ~ 15% kyanite and ~ 40% of other phases, largely amorphous aluminosilicate with significant Ti, Mg and alkalis (Yang et al. 2007). Phases present in much smaller amounts include native Fe; TiO_2 II, a high-pressure polymorph of rutile with the αPbO_2 structure; boron carbide of unknown stoichiometry; amorphous carbon; osbornite (TiN); and qingsongite (see Fig. 1), as well as Ti-Si-O and Ti-Al-Si-O grains that are too tiny to be identified (Yang et al. 2007). Coesite forms prisms several tens of μm long, but is polycrystalline, and thus interpreted to be pseudomorphs formed after the inversion of stishovite (Yang et al. 2007). One of the remarkable features of coesite (Fig. 6 a) is the presence of twin lamellae, which suggests that coesite had been subjected to local stress. However, the origin of the stress is not known – possibilities include stress during crystal growth and stress resulting from the volume change during transformation of stishovite to coesite. Twin lamellae are also present in kyanite (Fig. 6 b).

Qingsongite occurs either as inclusions in coesite that also contains inclusions of osbornite (Fig. 2 a), in osbornite enclosed in coesite (see Fig. 4 in Dobrzhinetskaya et al. 2009), or as isolated domains together with osbornite and amorphous carbon enclosed in kyanite.

Conditions of formation and origin

Our initial finding of coesite-kyanite intergrowths together with Fe-Ti alloy and microdiamond in OsIr alloy, which are inclusions in massive chromite ore from the mantle section of a Tibetan ophiolite, led us to conclude that such mineral associations require minimum pressure of 2.8 - 4 GPa (Yang et al. 2007). However, microstructures of the coesite prisms indicate that they are pseudomorphic after stishovite, implying a pressure > 9 GPa. These findings in what appears to be an unmetamorphosed mantle section of ophiolite were startling. The presence of TiO2 II confirms the stishovite interpretation because at 1300˚C, stability of TiO2 II requires a pressure

within the stishovite field (Whithers et al. 2003). The simplest scenario to explain these mineral assemblages is that at least some parts of the rootless podiform chromitites within the Luobusa ophiolite have a deeper origin than was then understood. Further support of a deep upper mantle origin is provided by the presence of exsolution lamellae of coesite and clinopyroxene in chromite, which indicate that the chromite may have had a $CaFe_2O_4$-(Ca-ferrite)-structure (Yamamoto et al. 2009), a phase that is stable at pressures over 12.5 GPa (Chen et al. 2003; Green 2004). A deep upper mantle origin also has the advantage of explaining the presence of stishovite as a relic of deeply subducted sediment (e.g., Irifune et al. 1994; Dobrzhinetskaya and Green 2007).

Yang et al. (2007) hypothesized that an impact origin is also a possible alternative explanation for the ultrahigh-pressure phases. However, microstructures in the fragment are inconsistent with shock metamorphism of a crustal rock, i.e., microstructures of the coesite pseudomorphs of stishovite are unlike those reported for either stishovite or coesite in shock-metamorphosed quartz-bearing rocks in impact structures, such as Ries Crater, Germany (Stähle et al. 2008) and Vredefort Dome, South Africa (Martini 1991). A feature common to the shock metamorphosed rocks is the absence for direct conversion of stishovite to coesite, although coesite is later than stishovite. In addition, the N and C isotopic compositions of osbornite have a mantle signature (see below), which is not consistent with the entire fragment being crustal rock that had been subjected to shock metamorphism.

Our temperature estimate of ~1300 °C for the qingsongite-bearing fragment is based on our previous suggestion that after exhumation the fragment remained at a shallow level of the oceanic lithosphere (Dobrzhinetskaya et al. 2009). We are unable to re-confirm this estimate independently, because there are no diagnostic mineral assemblages that could be used as geothermometers in the studied sample. Instead, we consider the constraints imposed by available phase diagrams for the minerals in the fragment and consistent with this temperature and with the probable presence of a chromite polymorph having a Ca-ferrite structure in the chromitite hosting the fragment (Yamamoto et al. 2009). At T ~ 1300 °C, TiO_2 II and stishovite constrain the pressure to be at least ~10 GPa (Akaogi et al. 2011; Withers et al. 2003); similarly, the presence of kyanite instead of stishovite + corundum gives a maximum pressure of 14-15

GPa (Schmidt et al. 1997; Liu et al., 2006, cf. Irifune et al., 1995; Ono, 1999). Dobrzhinetskaya et al. (2009) suggested that by analogy with coesite, kyanite could have formed from breakdown of stishovite + corundum, in which case the presence of kyanite would not place an upper limit on pressure.

Qingsongite itself provides no new constraints to supplement those indicated by the other phases in the fragment. There are four polymorphs of BN: hexagonal – h-BN, rhombohedral r-BN, wurtzite – w-BN) and cubic (sphalerite/zincblende) – c-BN); both h-BN and r-BN have layer structures (sp2 bonding) and lower densities compared to w-BN and c-BN, which are characterized by sp3 bonding. Cubic-BN has been synthesized over a wide range of P-T conditions, namely from < 2 GPa to 60 GPa at temperatures ranging from 400 °C to about 3000 °C (e.g., Bundy and Wentorf 1963; Corrigan and Bundy 1975; Singh et al. 1995a, b; Setaka and Sato 1992; Demazeau et al. 1995; Will et al. 2000). Solozhenko (1995) calculated from the extensive experimental studies on the c-BN = h-BN transition (Fig. 7) that it occurred at a significantly lower pressure than had been determined by Bundy and Wentworth (1963) and cited by Corrigan and Bundy (1975). Kern et al. (1999) performed *ab initio* calculations of the transition that provided support for Solozhenko's (1995) "equilibrium diagram", but noted that small variations of the free energy can result in large shifts in the transition temperature. Will et al. (2000) performed experiments showing that c-BN is stable at relatively low pressures and that kinetics play a decisive role in the transformation h-BN ⇔ c-BN. Wang et al. (2004) and Wang and Yang (2005) suggested that synthesis of c-BN at pressures lower than indicated by Corrigan and Bundy (1975) could be attributed to surface tension of nanosized grains, the so-called nanosize-induced interior pressure on the Gibbs free energy of critical nuclei. Hu et al. (2011) calculated a phase diagram in which the triple point of c-BN, h-BN and liquid is shifted from the position shown in Figure 7 to about 2700 K and 1.5 GPa as crystal size decreases to 2 nm. In summary, whatever the interpretation of the stability range of c-BN, all of them fall within the range constrained by the other phases in the fragment of our studies.

Mössbauer spectroscopy of massive chromite ores, which the highly reduced qingsongite - bearing fragment was recovered from, gave $Fe^{3+}/\Sigma Fe = 0.42$ (Ruskov et al. 2010). Ruskov et al. (2010) explained the surprisingly high proportion of Fe^{3+} in the "reduced" massive ores by

stabilization of Fe^{3+} in a high-pressure polymorph of chromite deep in the upper mantle through a mechanism such as charge-coupled substitution or creation of oxygen vacancies, accompanied by Fe disproportionation to balance charge.

Nitrogen and carbon isotopes provide important constraints on the origin of qingsongite. Citing compositions of $\delta^{15}N = -0.4 \pm 3$ ‰ and $\delta^{13}C = +5 \pm 7$ ‰ in osbornite led Dobrzhinetskaya et al. (2009) to conclude that the N clearly had a mantle origin, and C could not be derived from organic material (Fig. 8). The high uncertainty in $\delta^{13}C$ is due to small amount of C in osbornite. This $\delta^{15}N$ is more negative than the composition generally accepted for the upper mantle (~ –5‰, e.g., Cartigny and Ader 2003) and with the N found in basaltic vesicles, but N in some peridotitic diamonds have $\delta^{15}N = -10$ per mil or less (Fuxian diamonds, see Javoy 1997; Cartingy et al., 1997). Most iron meteorites have a more negative signature ($\delta^{15}N = -50$ ‰ to –90‰, Prombo and Clayton, 1993). These systematics are consistent with the N in our sample containing a component coming from deep in the mantle, or conceivably even from the core.

The protolith of the coesite-kyanite fragment containing qingsongite and osbornite inclusions probably has a crustal origin, because high contents of SiO_2 and Al_2O_3 are not typical for any known mantle reservoirs. The bulk composition of coesite + kyanite + amorphous material corresponds approximately to a mixture of SiO_2, Al_2SiO_5, $(K,Na)AlSi_3O_8$ and $MgTiO_3$, i.e., to a mixture of illite and other clays or muscovite with quartz, possibly with minor chlorite, assemblages characteristic of unmetamorphosed or low-grade pelitic metasediments. Non-pegmatitic muscovite is reported to contain 6-270 ppm B (Grew 2002) and illite and illite-clay mixtures, 23-~2000 ppm B (Lerman 1965; Reynolds 1965a,b; Couch and Grim 1968), sufficient for the formation of qingsongite if retained during deep subduction. The estimated composition differs from a typical pelite in having relatively high Ti content, absence of Fe and presence of N of mantle origin, i.e., the studied fragment is a hybrid consisting of crustal material "contaminated" by incorporation of mantle components.

Our proposed scenario (Fig. 9) starts with a pelitic sediment or low-grade metapelitic sediment that was subducted to mid-mantle depths as was previously conceptualized by Robinson et al. (2004). Yamamoto et al. (2009) presented evidence that the chromitite from which the fragment

was extracted had also been deeply buried. Yamamoto et al. (2013) reported spot analyses of zircons extracted from Luobusa podiform chromitite giving ages as old as Late Archean, and interpreted the zircons as xenocrysts entrained in chromitites after residing in mantle peridotite, that is, crustal contamination of upper mantle under the Neo-Tethys Ocean. As regards metamorphism of the fragment during deep subduction, experiments on pelitic sediments, basalt and andesite, the high-Si variety of muscovite, phengite, would remain stable until deeply buried, and only at 9-11 GPa would break down to K-hollandite, a high-pressure form of $(K,Na)AlSi_3O_8$ (e.g., Schmidt 1996; Domanik and Holloway 1996, 2000). Yang et al. (2007) cited a microstructural similarity between the coesite psudomorphs in the fragment and stishovite prisms crystallizing with K-hollandite from a 50% SiO_2 and 50% $KAlSi_3O_8$ mixture at T = 900 °C, P = 10 GPa, in an experimental run by Dobrzhinetskaya and Green (2007). At this juncture, interaction with the highly reducing environment and Fe-Ti metal in the mantle could have resulted in the anomalous compositional features of the fragment. For example, oxygen fugacity could be so low that Fe^{2+} in silicate minerals or melt is no longer stable and iron separates out as Fe metal, leaving the fragment depleted in Fe. Under the highly reducing conditions, mantle N combined with Ti and B to form osbornite and qingsongite, respectively. The age of osbornite and qingsongite formation is not tightly constrained. These minerals could have formed over 500 Ma ago when crustal materials were subducted into the mantle, according to the scenario for tectonic evolution suggested by Yamamoto et al. (2013). However, a more plausible estimate is given by the depleted Os-model age of 234±3 Ma for a component of the podiform chromitites (Shi et al. 2007; Yamamoto et al. 2009). This component together with ultrahigh-pressure minerals were transported upward by mantle upwelling most likely prior to the first stage of formation of the ophiolite and podiform chromitite at ca. 170 Ma, but certainly before ca. 120 Ma, the age of supra-subduction magmatism dated by zircon (Robinson et al. 2004; Yamamoto et al. 2009, 2013); i.e., the range 120-170 Ma is the minimum possible age for osbornite and qingsongite in the Luobusa chromitite.

The inversion of stishovite to coesite involves a substantial volume increase (over 40% from volumes measured at room temperature and 1 bar pressure). However, except for the lamellar twinning in coesite and kyanite (Fig. 6 a, b), and possible dislocations in coesite (see left upper corner of image on Fig 6 a), no other microstructures related to deformation or volume change

were observed during our studies of the nitrides-coesite-kyanite-bearing fragment. Possibly, the neighboring amorphous phase accommodated the strain through plastic deformation or Si diffused out of the fragment into the neighboring Fe-Ti alloy, a possibility suggested by the narrow zone (<1 μm) of Si-Al alloy between the aluminosilicate fragment and native Ti bordering the Fe-Ti alloy (Fig. 1). As noted by Dobrzhinetskaya et al. (2009), coesite did not invert to quartz during later stages of exhumation as most likely water fugacity was too low.

In summary, qingsongite has a mixed parentage – B most likely crustal, but N most likely mantle, nonetheless, qingsongite is a mantle mineral, because it is composed of mantle N combined with B under highly reducing conditions. Such a combination is not a surprise for a crustal material that once, at least, was deeply subducted and then exhumed back to the shallow levels of Earth. For example, Sumino et al (2011) showed that in the Kokchetav massif, Kazakhstan, microdiamonds crystallized from crustal carbon and enclosed in crustal ultrahigh pressure metamorphic rocks subducted to a depth of ~210 km, contain inclusion-hosted $^{3}He/^{4}He$ of $(3.3–6.5)\times10^{-5}$. This range of $^{3}He/^{4}He$ ratio is close to that of noble gases enriched in a primordial component and delivered from the deep mantle by plumes to oceanic island environments, i.e., the Kokchetav diamond-bearing rocks were “hybridized” with the mantle components. By analogy, we suggest that the qingsongite-bearing fragment has both crustal and mantle geochemical characteristics.

Our discovery of qingsongite in the Luobusa ophiolite, together with the discoveries of osbornite, coesite pseudomorphs of stishovite discovered by Yang et al. (2007) and Dobrzhinetskaya et al. (2009), coesite exsolution lamellae in chromite (Yamamoto et al., 2009) and Archean zircons by Yamamoto et al. (2013), have important implications for our current understanding of the process and depths of formation of podiform chromitites in the mantle sections of ophiolites, since these have now been shown to contain mineral assemblages indicative of deep subduction of crustal material.

Acknowledgments

We thank S. Yamamoto, and Y. Sano (The University of Tokyo, Japan) and S. Maruyama (The Tokyo Institute of Technology, Japan) for their fruitful discussions of the significance of

ultrahigh-pressure minerals in mantle section of ophiolite and nitrogen reservoirs in deep Earth. L. Dubrovisnky and A. El Goresi (The University of Bayreuth, Germany) are acknowledged for stimulating discussions of the laboratory synthesis and conditions for natural formations of the osbornite and cubic boron nitride. Members of the IMA Commission on New Minerals, Nomenclature and Classification are thanked for their comments on the new-mineral proposal submitted for approval by the commission. Monika Koch-Müller and an anonymous reviewer are thanked for their constructive comments on an earlier version of the manuscript. The project was supported by the NSF grant EAR #1118796 to LFD and HWG, and the Lab Fee Research Award (No. 09-LR-05-116946-DOBL) from the University of California to LFD, HWG, IDH and PKW. The research is also a part of the activity of Task Force IV of the International Lithosphere Program. The portion of the study related to sample collection and heavy minerals separation was partially supported by the Chinese National Science Foundation and the China Geological Survey to JSY.

REFERENCES

Akaogi, M., Oohata, M., Hojitani, H. and Kawaji, H. (2011) Thermodynamic properties of stishovite by low-temperature heat capacity measurements and the coesite-stishovite transition boundary. American Mineralogist, 96, 1325–1330.

Arblaster, J.W. (1997) Crystallographic properties of platinum. Platinum Metals Review, 41, 12-21.

Bogdanov, S.P. (2008) Influence of boron impurities on the crystal structure of cubic boron nitride. Glass Physics and Chemistry, 34, 218-223.

Bundy, F.P. and Wentorf, R.H. (1963) Direct transformation of hexagonal boron nitride to denser forms. Journal of Chemical Physics, 38, 1144-1149.

Cartigny, P. and Adar, M. (2003) A comment on ‘‘The nitrogen record of crust–mantle interaction and mantle convection from Archean to Present’’ by B. Marty and N. Dauphas [Earth and Planetary Science Letters (2003) 206, 397-410] Earth and Planetary Science Letters, 216, 425-432.

Cartigny, P., Boyd, S.R., Harris, J.W. and Javoy, M. (1997) Nitrogen isotopes in peridotitic diamonds from Fuxian, China: the mantle signature. Terra Nova, 9, 175-179.

Chen, M., Shu, J., Mao, H.K., Xie, X. and Hemley, R.J. (2003) Natural occurrence and synthesis of two new postspinel polymorphs of chromite. Proceedings of the National Academy of Sciences, 100, 14651–14654.

Corrigan, F.R. and Bundy, F.P. (1975) Direct transitions among the allotropic forms of boron nitride at high pressures and temperatures. Journal of Chemical Physics, 63, 3812-3820.

Couch, E.L. and Grim, R.E. (1968) Boron fixation by illites. Clays and Clay Mineral, 16, 249-256.

Day, H.W. (2012) A revised diamond-graphite transition curve. American Mineralogist, 97, 53-62.

Demazeau, G., Gonnet, V., Solozhenko, V., Tanguy, B. and Montigaud, H. (1995) BN-cubique: une nouvelle voie d'élaboration à moyenne pressions et temperatures. Comptes Rendus de l'Académie des Sciences de Paris, 320, Série IIb, 419-422.

Dobrzhinetskaya, L.F., and Green, H.W. (2007) Experimental studies of mineralogical assemblages of metasedimentary rocks at Earth's mantle transition zone conditions: Journal of Metamorphic Geology, 25, 83-96.

Dobrzhinetskaya, L.F., Wirth, R., Yang, J., Hutcheon, I.D., Weber, P.K. and Green, H.W. II (2009) High-pressure highly reduced nitrides and oxides from chromitite of a Tibetan ophiolite. Proceedings of the United States National Academy of Sciences, 106, 19233-19238.

Dobrzhinetskaya L.F., Green, H. W., Takahata, N., Sano, Y. and Shirai, K. (2010) Crustal signature of $\delta^{13}C$ and nitrogen content in microdiamonds from Erzgebirge, Germany: Ion microprobe studies. Journal of Earth Sciences, 21, 623–634.

Dobrzhinetskaya, L.F., Wirth, R., Yang, J., Green, H.W., II, Hutcheon, I.D., Weber, P.K. and Grew, E.S. (2013) Qingsongite, IMA 2013-030. CNMNC Newsletter No. 16, August 2013, page 2708. Mineralogical Magazine, 77, 2695-2709.

412 Domanik, K.J. and Holloway, J.R. (1996) The stability and composition of phengitic muscovite
413 and associated phases from 5.5 to 11 GPa: Implications for deeply subducted sediments.
414 Geochimica et Cosmochimica Acta, 60, 4133-4150.

415 Domanik, K.J. and Holloway, J.R. (2000) Experimental synthesis and phase relations of
416 phengitic muscovite from 6.5 to 11 GPa in a calcareous metapelite from the Dabie
417 Mountains, China. Lithos, 52, 51-77.

418 Eichhorn, K., Kirfel, A., Grochowski, J. and Serda, P. (1991) Accurate structure analysis with
419 synchrotron radiation. An application to borazone, cubic BN. Acta Crystallographica, B47,
420 843-848.

421 Gaillou, E., Post, J.E., Rost, D. and Butler, J.E. (2012) Boron in natural type IIb blue diamonds:
422 Chemical and spectroscopic measurements. American Mineralogist, 97, 1-18.

423 Gardinier, C.F. (1988) Physical properties of superabrasives. Ceramic Bulletin, 67, 1006-1009

424 Gielisse, P.J., Mitra, S.S., Plendl, J.N., Griffis, R.D., Mansur, L.C., Marshall, R. and Pascoe,
425 E.A. (1967) Lattice infrared spectra of boron nitride and boron monophosphide. Physical
426 Review, 155, 1039-1046.

427 Green, H. (2004) Shock-induced minerals in meteorite provide prospecting tools for mineral
428 physics. Proceedings of the United States National Academy of Sciences, 101, 6–7.

429 Grew, E.S. (2002) Borosilicates (exclusive of tourmaline) and boron in rock-forming minerals in
430 metamorphic environments. In Grew, E.S. and Anovitz, L.M. (eds), Boron: Mineralogy,
431 Petrology and Geochemistry. Mineralogical Society of America, Reviews in Mineralogy,
432 33, 389-502.

433 Haubner, R., Wilhem, M., Weissenbacher, R. and Lux, B. (2002) Boron nitrides – Properties,
434 synthesis and applications. Structure and Bonding, 102, 1-45

435 Hemingway, B.S., Bohlen, S.R., Hankins, W.B., Westrum, E.F. Jr. and Kuskov, O.L. (1998)
436 Heat capacity and thermodynamic properties for coesite and jadeite, reexamination of the
437 quartz-coesite equilibrium boundary. American Mineralogist, 83, 409–418.

Horvath-Bordon, E., Ralf Riedel, R., Zerr, A.,. McMillan, P.F., Prots, Y., Bronger, W., Kniep, R. and Kroll, P. (2006) High-pressure chemistry of nitride-based materials. Chemical Society Reviews, 35, 987-1014.

Howe, J.Y., Rawn, C.J., Jones, L.E. and Ow, H. (2002) Improved crystallographic data for graphite. Powder Diffraction, 18, 150-154.

Hu, S., Yang, J. Liu, W., Dong, Y. Cao, S. and Liu, J. (2011) Prediction of formation of cubic boron nitride by construction of temperature−pressure phase diagram at the nanoscale. Journal of Solid State Chemistry, 184, 1598–1602.

Irifune, T., Ringwood, A.E. and Hibberson, W.O. (1994) Subduction of continental crust and terrigenous and pelagic sediments: an experimental study. Earth and Planetary Sciences, 126, 351-368.

Irifune T, Kuroda K, Minagawa T, Unemoto M (1995) Experimental study of the decomposition of kyanite at high pressure and high temperature. In: Yukutake T (ed) The Earth's central part: its structure and dynamics. Terra Scientific publishing, Tokyo, pp 35–44

Irifune, T., Kurio, A., Sakamoto, S., Inoue, T. and Sumiya, H. (2003) Materials: Ultrahard polycrystalline diamond from graphite. Nature, 421, 599-600.

Javoy, M. (1997) The major volatile elements of the Earth: Their origin, behavior, and fate. Geophysical Research Letters, 24, 177-180.

Kern, G., Kresse, G. and Hafner, J. (1999) Ab initio calculation of the lattice dynamics and phase diagram of boron nitride. Physical Review B, 59, 8551–8559.

Leeman W. P. and Sisson V. B. (2002) Geochemistry of boron and its implications for crustal and mantle processes. In Grew, E.S. and Anovitz, L.M. (eds), Boron: Mineralogy, Petrology and Geochemistry. Mineralogical Society of America, Reviews in Mineralogy, 33, 645-707.

Lerman, A. (1965) Boron in clays and estimation of paleosalinities. Sedimentology, 6, 267-286.

Liu, X., Nishiyama, N., Sanehira, T., Inoue, T., Higo, Y. and Sakamoto, S. (2006) Decomposition of kyanite and solubility of Al_2O_3 in stishovite at high pressure and high temperature conditions. Physics and Chemistry of Minerals, 33, 711-721.

Lodders, K. (2010) Solar system abundances of the elements. In: A. Goswami and B.E. Reddy (eds.), Principles and Perspectives in Cosmochemistry. Astrophysics and Space Science Proceedings. Springer-Verlag, Berlin Heidelberg, p. 379-417.

Martini, J.E.J. (1991) The nature, distribution and genesis of the coesite and stishovite associated with the pseudotachylite of the Vredefort Dome, South Africa. Earth and Planetary Science Letters, 103, 285-300.

Ono, S. (1999) High temperature stability limit of phase egg, $AlSiO_3(OH)$. American Mineralogist, 137, 83–89.

Palme, H and O'Neill, H. St. C. (2005): Cosmochemical estimates of mantle composition. In: Carlson, R.W., ed., The Mantle and Core, Vol. 2, Holland, H.D. & Turekian, K.K., eds., Treatise on Geochemistry, p. 1-38. Elsevier-Pergamon, Oxford.

Palot, M., Cartigny, P., Harris, J.W., Kaminsky, F.V. and Stachel, T. (2012) Evidence for deep mantle convection and primordial heterogeneity from nitrogen and carbon stable isotopes in diamond. Earth and Planetary Science Letters, 357-358, 179-193.

Prombo, C.A. and Clayton, R.N. (1993) Nitrogen isotopic compositions of iron meteorites. Geochimica et Cosmochimica Acta, 57, 3749-3761.

Reynolds, R.C., Jr. (1965a) The concentration of boron in Precambrian seas. Geochimica et Cosmochimica Acta, 29, 1-16.

Reynolds, R.C., Jr. (1965b) Geochemical behavior of boron during the metamorphism of carbonate rocks. Geochimica et Cosmochimica Acta, 29, 1101-1114.

Robinson, P.T., Bai, W.-J., Malpas, J., Yang, J.-S., Zhou, M.F., Fang, Q.-S., Hu, X.-F., Cameron, S. and Staudigel, H. (2004) Ultra-high pressure minerals in the Luobusa Ophiolite, Tibet, and their tectonic implications. In: Malpas, J., Fletcher, C.J.N., Ali, J.R. and Aitchison, J.C.

(eds), Aspects of the Tectonic Evolution of China. Geological Society, London, Special Publications, 226, 247-271.

Rudnik, R.L. and Gao, S. (2005) Composition of the continental crust. In Rudnick, R.L. (ed.) The Crust, volume 3 of Holland, H.D. and Turekian, K.K. (eds.) Treatise on Geochemistry, p. 1-64. Elsevier-Pergamon, Oxford.

Ruskov, T., Spirov, I., Georgieva, M., Yamamoto, S., Green, H.W., McCammon, C.A. and Dobrzhinetskaya, L.F. (2010) Mössbauer spectroscopy studies of the valence state of iron in chromite from the Luobusa massif of Tibet: implications for a highly reduced deep mantle. Journal of Metamorphic Geology, 28, 551-560.

Schmidt, M.W. (1996) Experimental constraints on recycling of potassium from subducted oceanic crust. Science, 272, 1927-1930.

Schmidt, M.W., Poll, S., Comodi, P. and Zanazzi, P.F. (1997) High-pressure behavior of kyanite: Decomposition of kyanite into stishovite and corundum. American Mineralogist, 82, 460-466.

Setaka, N. and Sato, T. (1992) Diamond and cubic boron nitride synthesis by means of shock-compression. In Sawaoka, A.B. (eds) Shock Compression Technology and Material Science, p. 87-102. KTK Scientific Publishers / Terra Scientific Publishing Company, Tokyo.

Shi, R., Alard, O., Zhi, X., O'Reilly, S.Y., Pearson, N.J., Griffin, W.L., Zhang, M. and Chen, X. (2007) Multiple events in the Neo-Tethyan oceanic upper mantle: Evidence from Ru–Os–Ir alloys in the Luobusa and Dongqiao ophiolitic podiform chromitites, Tibet. Earth and Planetary Science Letters, 261, 33-48.

Smith, D.G.W. and Nickel, E.H. (2007) A System of Codification for Unnamed Minerals: Report of the SubCommittee for Unnamed Minerals of the IMA Commission on New Minerals, Nomenclature and Classification. Canadian Mineralogist, 45, 983-1055.

Singh, B.P., Solozhenko, V.L. , Will, G. (1995a) On low pressure synthesis of cubic boron nitride. Diamond and related materials, 4, 1193-1196.

Singh, B.P., Nover, G. and Will, G. (1995b) High pressure phase transformations of cubic boron nitride from amorphous boron nitride using magnesium boron nitride aas as the catalyst. Journal of Crystal Growth, 152, 143-149.

Solozhenko, V.L. (1995) Current trends in the phase-diagram of boron nitride. Journal of Hard Materials, 6, 51-65.

Solozhenko, V.L., Chernyshev, W., Fetisov, G.V., Ryabakov, V.B. and Petrusha, I.A. (1990) Structure-analysis of the cubic-nitride crystals. Journal of Physics and Chemistry of Solids, 51, 1011-1012.

Soma, T., Sawaoka, A. and Saito, S. (1974) Characterization of wurtzite type boron nitride synthesized by shock compression. Materials Research Bulletin, 9, 755-762.

Stähle, V., Altherr, R., Koch, M. and Nasdala, L. (2008) Shock-induced growth and metastability of stishovite and coesite in lithic clasts from suevite of the Ries impact crater (Germany). Contributions to Mineralogy and Petrology, 155, 457-472.

Sumino, H., Dobrzhinetskaya, L.F., Burgess, R. and Kagi, H. (2011) Deep-mantle-derived noble gases in metamorphic diamonds from the Kokchetav massif, Kazakhstan. Earth and Planetary Science Letters, 307, 439-440.

Urakawa, S., Kondo, T. Igawa, N., Shimomura, O. and Ohno, H. (1994) Synchrotron radiation study on the high-pressure and high-temperature phase relations of $KAlSi_3O_8$. Physics and Chemistry of Minerals, 21, 387-391.

Vel, L., Demazeau, G. and Etourneau, J. (1991) Cubic boron nitride: synthesis, physicochemical properties and applications. Materials Science and Engineering, B10, 149-164.

Wang, C.X. and Yang, G.W. (2005) Thermodynamics of metastable phase nucleation at the nanoscale. Materials Science and Engineering Reports, 49, 157–202.

Wang, X.C., Jia, X.P, Zhan, T.C., Ren, G.Z., Liu, H.J., Zang, C.Y., Zhu, P.W., Ma, H.A. and Zou, G.T. (2003) cBN synthesis in the system of hBN–Mg and bonded water. Diamond and Related Materials, 12, 57–60.

Wang, C.X., Yang, Y.H., and Yang, G.W. (2004) Nanothermodynamic analysis of the low-threshold-pressure-synthesized cubic boron nitride in supercritical-fluid systems. Applied Physics Letters, 84, 3034-3036.

Wentorf, R.H. (1957) Cubic form of boron nitride. Journal of Chemical Physics, 26, 956.

Wentorf, R.H. (1961) Synthesis of the cubic form of boron nitride. Journal of Chemical Physics, 34, 809-812.

Will, G., Kirfel, A. and Josten B. (1986) Charge density and chemical bonding in cubic boron nitride. Journal of the Less Common Metals, 117, 61-71.

Will, G., Nover, G. and von der Gönna, J. (2000) New experimental results on the phase diagram of boron nitride. Journal of Solid State Chemistry, 154, 280-285.

Withers, A.C., Essene, E.J. and Zhang, Y. (2003) Rutile/TiO_2II phase equilibria. Contributions to Mineralogy and Petrology, 145, 199-204.

Yamamoto, S., Komiya, T., Hirose, K. and Maruyama S (2009) Coesite and clinopyroxene exsolution lamellae in chromites: In situ ultrahigh-pressure evidence from podiform chromitites in the Luobusa ophiolite, southern Tibet. Lithos. 109, 314–322.

Yamamoto, S., Komiya, T., Hirose, K., Kaneko, Y., Terabayashi, M., Katayama, I., Iizuka, T., Maruyama, S., Yang, J., Kon, Y. and Hirata, T. (2013) Recycled crustal zircons from podiform chromitites in the Luobusa ophiolite, southern Tibet. Island Arc, 22, 89–103.

Yang, J.-S., Dobrzhinetskaya, L.F., Bai, W.J., Fang, Q.-S., Robinson, P.T., Zhang, J. and Green, H.W. II (2007) Diamond- and coesite-bearing chromitites from the Luobusa ophiolite, Tibet. Geology, 35, 875-878.

Figure captions

Figure 1. Scanning electron microscope images of the rock sample containing qingsongite (from Dobrzhinetskaya et al., 2009). (a) back-scattered electron image of Fe–Ti pellet rimmed by silicate rock (boxed area); (b) detail of the boxed area shows silicate material containing coesite (coe), kyanite (ky), qings (qingsongite), unknown amorphous phase (*) of

the composition: (SiO_2 - 63.00, Al_2O_3 -14.50, TiO_2 - 9.02, CaO - 0.5, MgO - 4.26, K_2O - 5.16, in wt. %) and osbornite (bright spots).

Figure 2. (a): a part of the TEM foil exhibits coesite matrix (light grey contrast), osbornite (TiN, bright contrast), qingsongite (c-BN, darker grey contrast) (modified from Dobrzhinetskaya et al., 2009); (b): energy dispersive X ray spectrum shows presence of intense peaks for boron – B and nitrogen – N (inclusion of qingsongite) considering the small fluorescence yields of boron and nitrogen; Ga-peak originates from Ga-implantation during the TEM foil preparation with FIB; Cu X-ray intensity - from the TEM Cu-grid; Si and O X-ray intensities are from matrix coesite and Ti is from neighboring osbornite.

Figure 3. EEL-spectra: (a) boron K-edge with the edge onset at 189 eV and (b) nitrogen K-edge with the edge onset at 409 eV.

Figure 4. EDX element maps of the area boxed on Fig. 2. (a) an image of the mapped area, (b) boron, (c) nitrogen, (d) nitrogen, (e) silicon, (f) oxygen.

Figure 5. A high-resolution lattice fringe image of BN (a) with the corresponding diffraction pattern (FFT) (b). The 220-reflections are weak (their positions are pointed by open circle) because the [100] zone axis is not perfectly aligned parallel to the electron beam.

Figure 6. TEM images showing: (a) – Bright field image of coesite with twin lamellae containing an inclusion of osbornite; (b) – HAADF image with twin lamellae in kyanite (white arrows) containing inclusions of osbornite and TiO_2 II.

Figure 7. Boron nitride phase diagram modified from Solozhenko (1995). 1. Dashed line based on Bundy and Wentworth (1963) is essentially the same as reported by Corrigan and Bundy (1975). 2. Solid line is based on the "equilibrium diagram" derived by Solozhenko et al. (1990). The c-BN – h-BN – liquid triple point is marked by a circle.

Figure 8. Nitrogen isotope characteristics of crustal and mantle materials (modified from Javoy, 1997).

Figure 9. Pressure-Temperature diagram showing reactions relevant to the formation conditions and origin of qingsongite. Sources of data: Hexagonal-BN (h-BN) ↔ c-BN (Corrigan and

Bundy 1975); graphite ↔ diamond (Day 2012); reactions involving K-bearing phases in the system KAlSi3O8, dashed where some experimental constraints and dotted where estimated (simplified from Urakawa et al. 1994); coesite ↔ stishovite (Akaogi et al. 2011); rutile ↔ rutile II (Withers et al. 2003); kyanite ↔ stishovite + corundum (Schmidt et al. 1997); coesite ↔ quartz, dashed where extrapolated (Hemingway et al. 1998). Boxes and arrows mark the evolution of the qingsongite-bearing fragment.

Table 1. Calibrations of the fast Fourier transforms from high-resolution images internal standards.

hkl	d_{hkl} observed (Å)	d_{hkl} calculated from literature (Å)	|Δ| (Å)[a]
		Platinum[b]	
111	2.222	2.2653	0.043
200	1.970	1.9618	0.008
		Graphite[c]	
10-11	1.927	2.0318	0.105
10-12	1.898	1.7994	0.099
0004	1.691	1.6777	0.013
11-22	1.157	1.1556	0.001
Average |Δ| (standard deviation)			0.045 (0.046)

Note: [a]|Δ| is the absolute value of the difference between observed and calculated d_{hkl}. [b]For a = 3.9236 Å (Arblaster 1997). [c]For a = 2.4617 Å, c = 6.7106 Å (Howe et al. 2002).

Table 2. Measured and calculated angles in qingsongite.

Planes (*hkl*)	angle between planes	
	observed	calculated[a]
(200)/(111)	54.80°	54.74°
(-111)/(111)	69.70°	70.53°
(200)/(1-1-1)	54.80°	54.74°

Note: [a]For a = 3.61 Å

Table 3. Powder X-ray diffraction data for synthetic qingsongite from Soma et al. (1974) for a = 3.6157 (10) Å.

I_{rel}	d_{meas} (Å)	d_{calc} (Å)	$h\ k\ l$
100	2.088	2.088	1 1 1
8	1.808	1.808	2 0 0
20	1.277	1.278	2 2 0
10	1.0903	1.0904	3 1 1
3	0.9040	0.9039	4 0 0
8	0.8296	0.8295	3 3 1

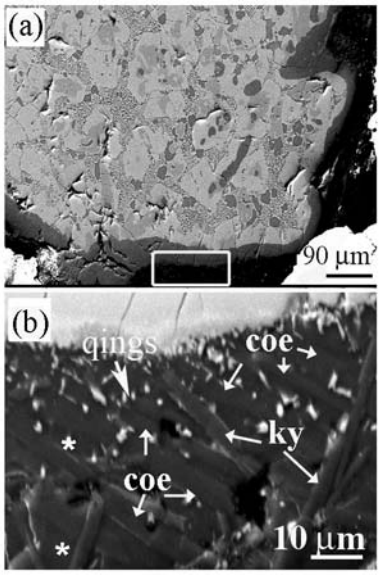
(a)
90 μm
(b)
qings
coe
ky
coe
10 μm

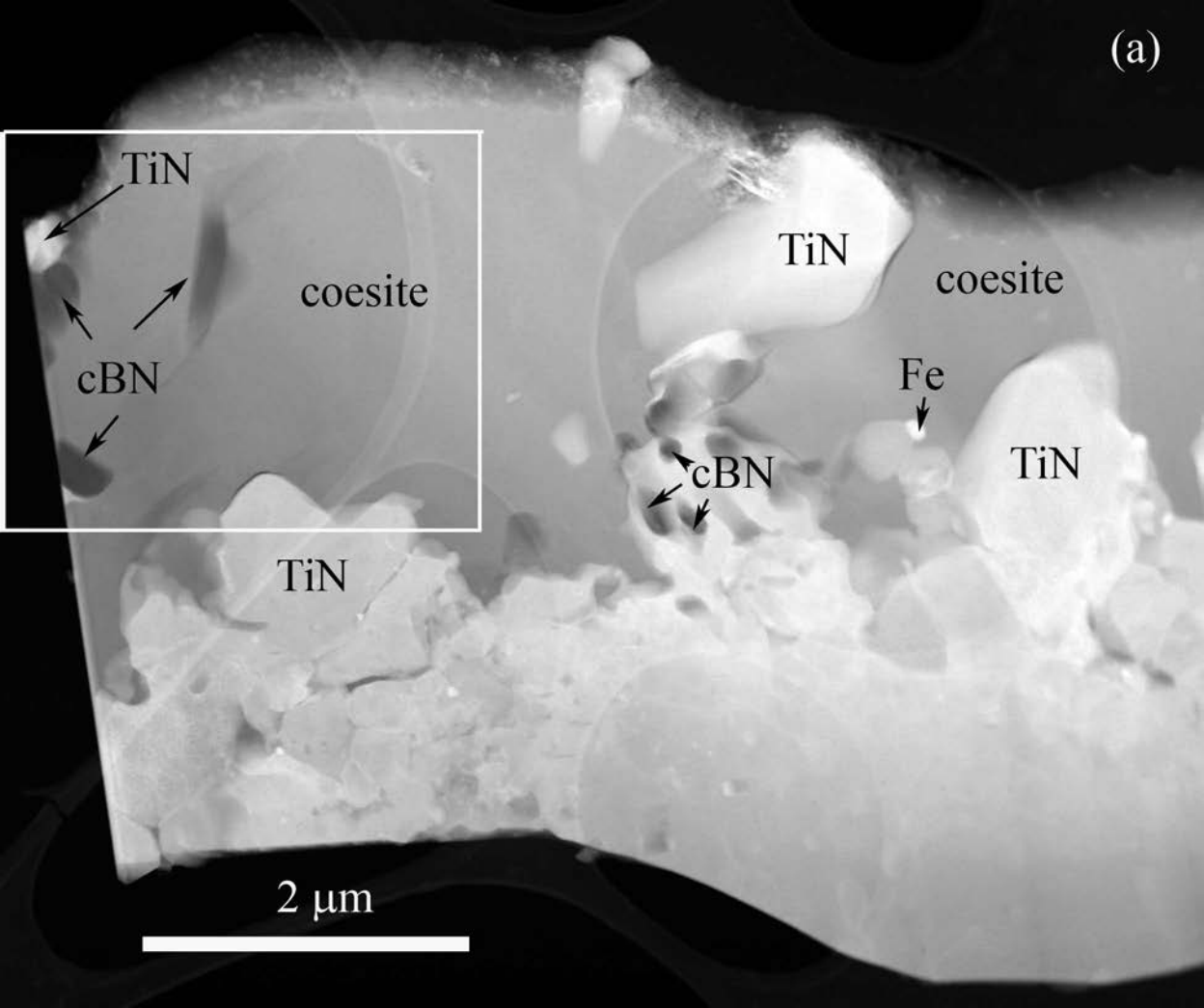
(a)
TiN
coesite
cBN
TiN
TiN
coesite
Fe
cBN
TiN
2 μm

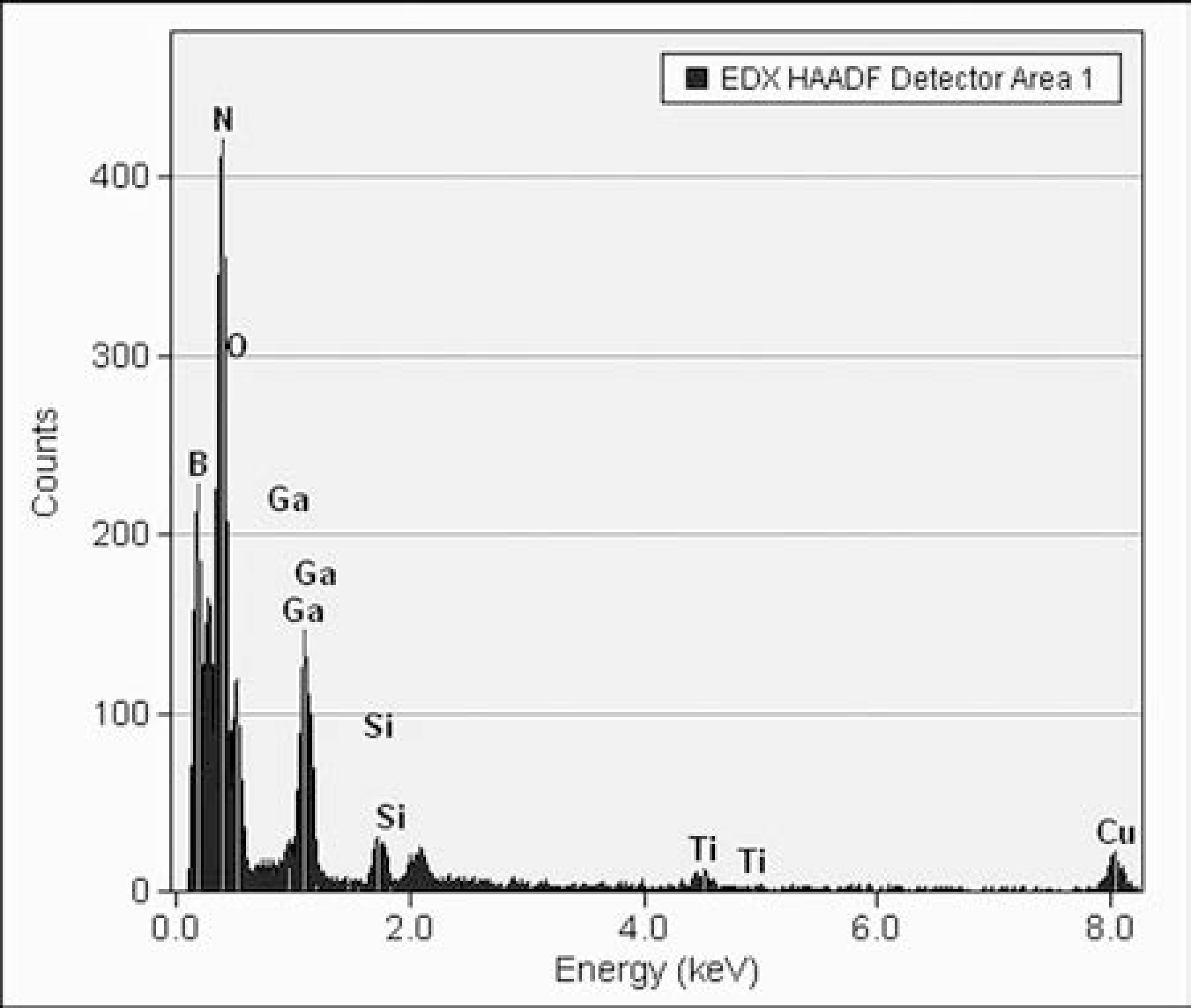
EDX HAADF Detector Area 1
N
O
B
Ga
Ga
Ga
Si
Si
Ti
Ti
Cu
400
300
200
100
0
Counts
0.0
2.0
4.0
6.0
8.0
Energy (keV)

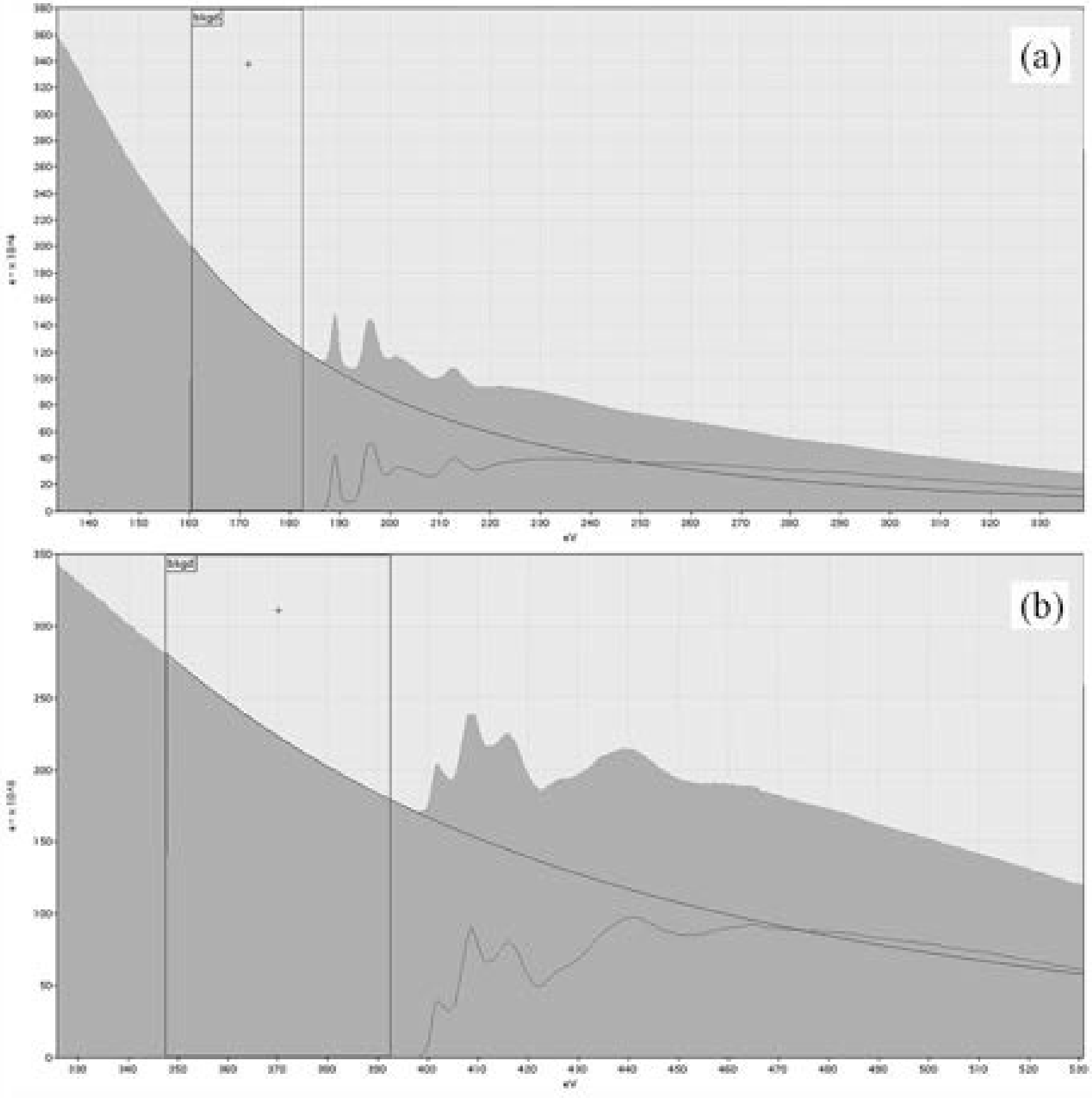
(a)
(b)
eV

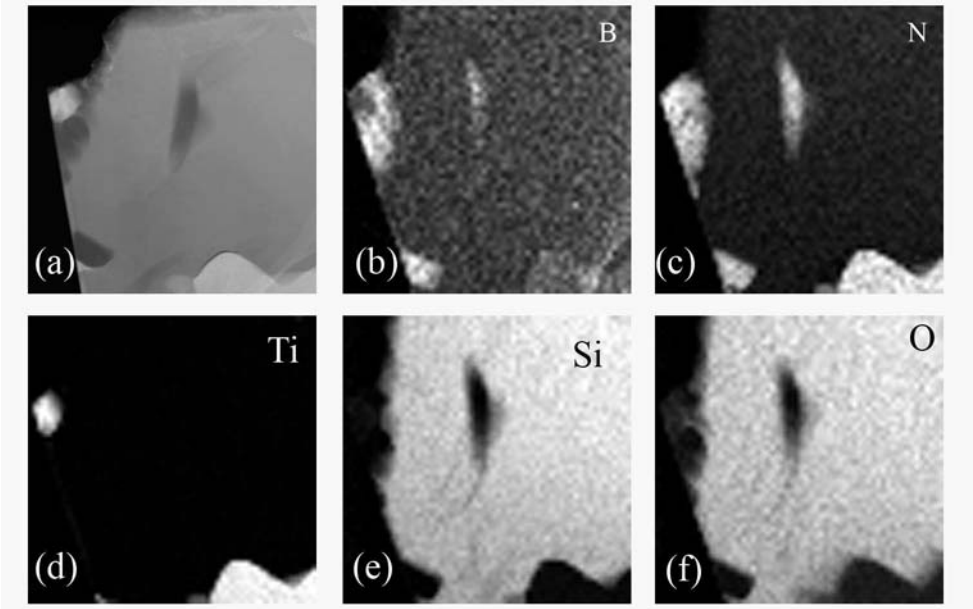
(a)
B
(b)
N
(c)
Ti
(d)
Si
(e)
O
(f)

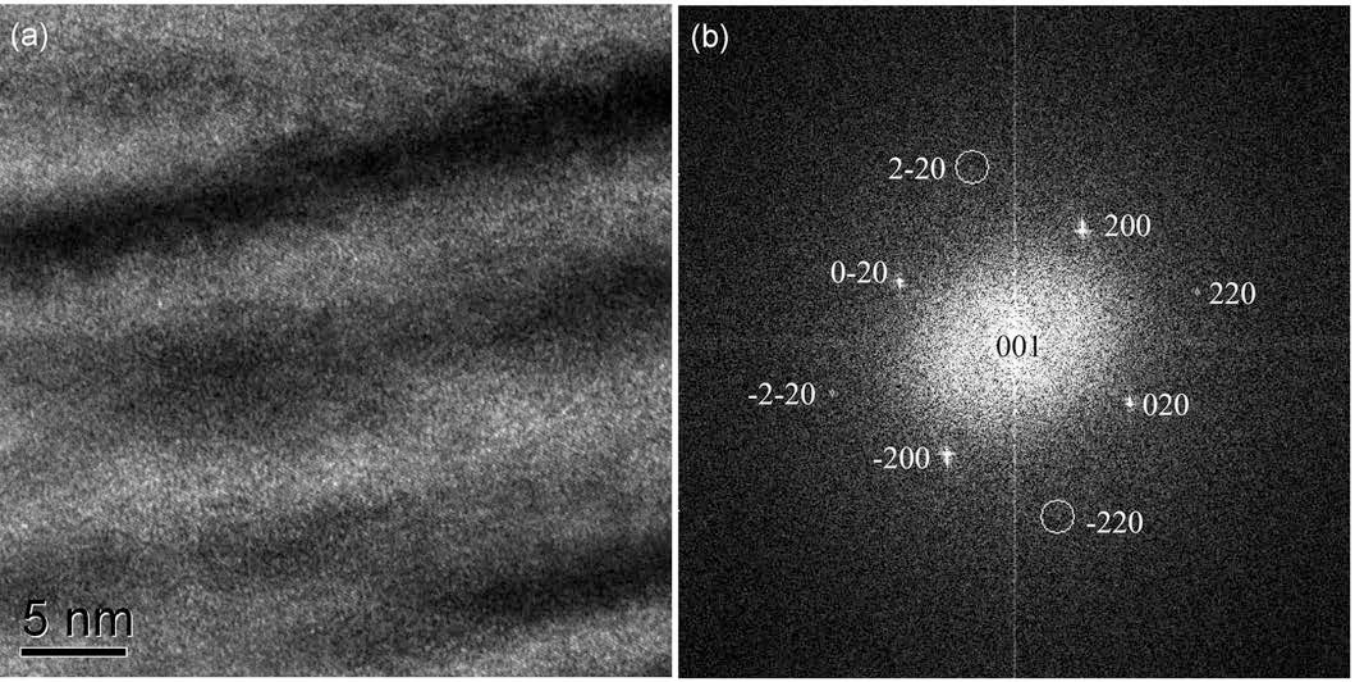
(a)
5 nm
(b)
2-20
200
0-20
220
001
-2-20
020
-200
-220

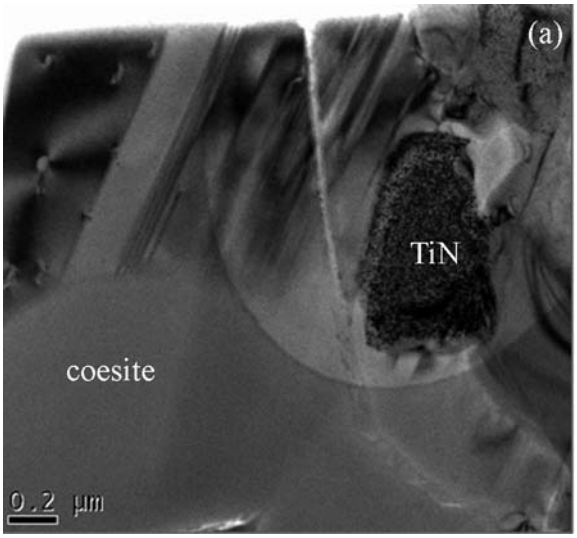
(a)
TiN
coesite
0.2 μm

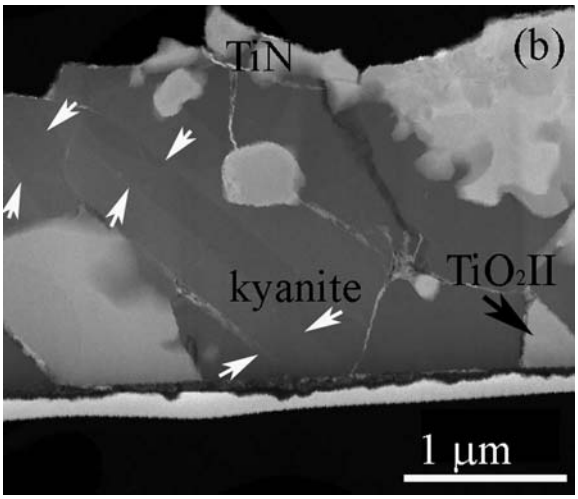
TiN
(b)
kyanite
TiO2II
1 μm

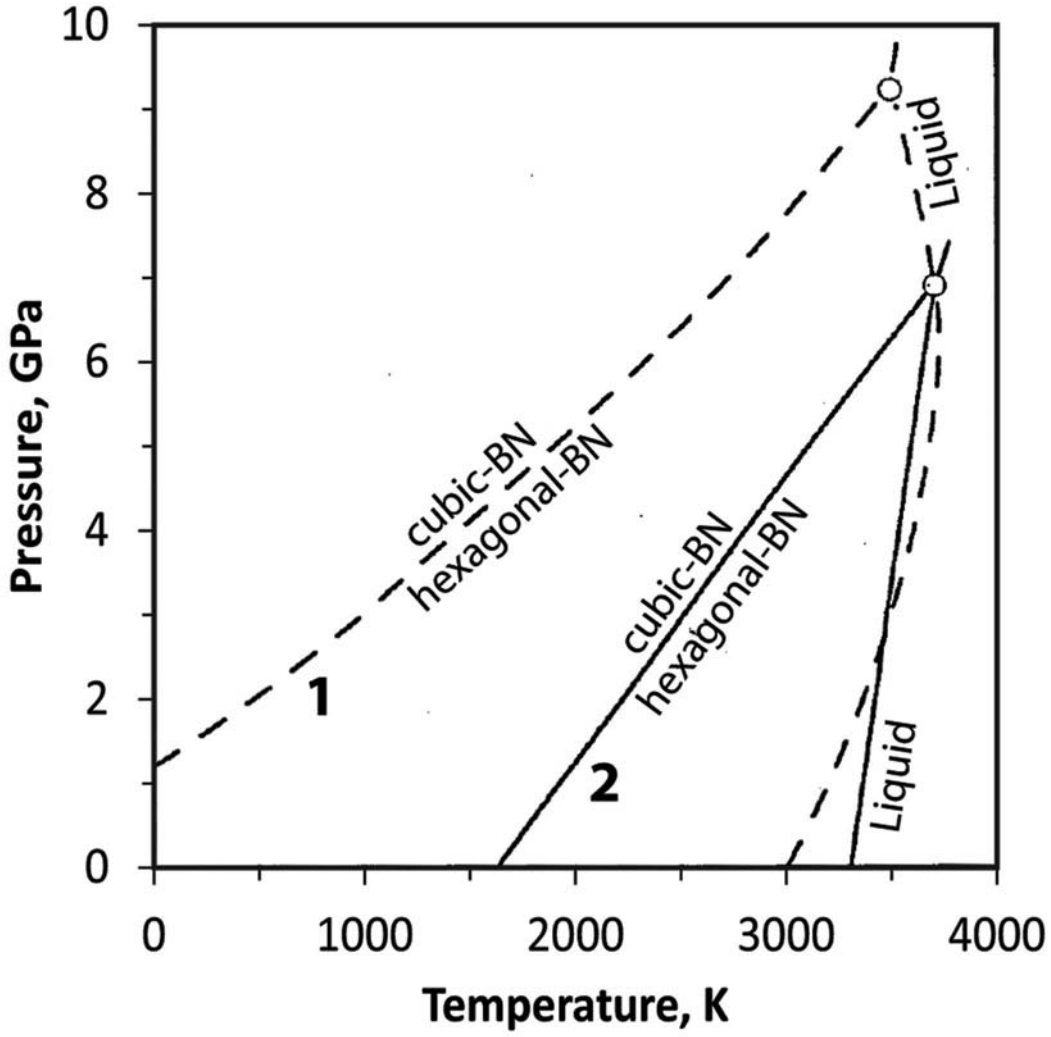
10
8
6
4
2
0
Pressure, GPa
0
1000
2000
3000
4000
Temperature, K
cubic-BN
hexagonal-BN
Liquid
1
cubic-BN
hexagonal-BN
2
Liquid

Figure 8

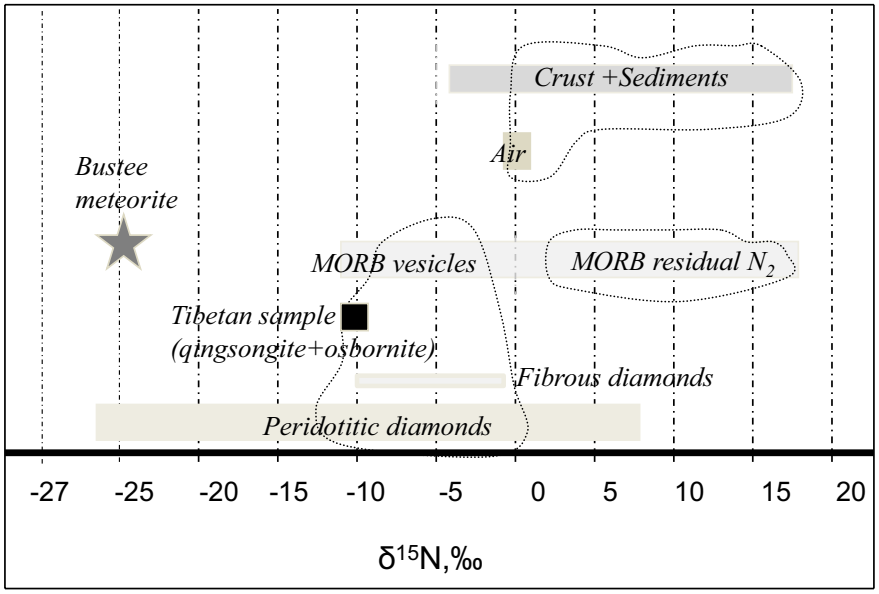
Crust +Sediments
Air
Bustee
meteorite
MORB vesicles
MORB residual N_2
Tibetan sample
(qingsongite+osbornite)
Fibrous diamonds
Peridotitic diamonds
-27
-25
-20
-15
-10
-5
0
5
10
15
20
$\delta^{15}N$,‰

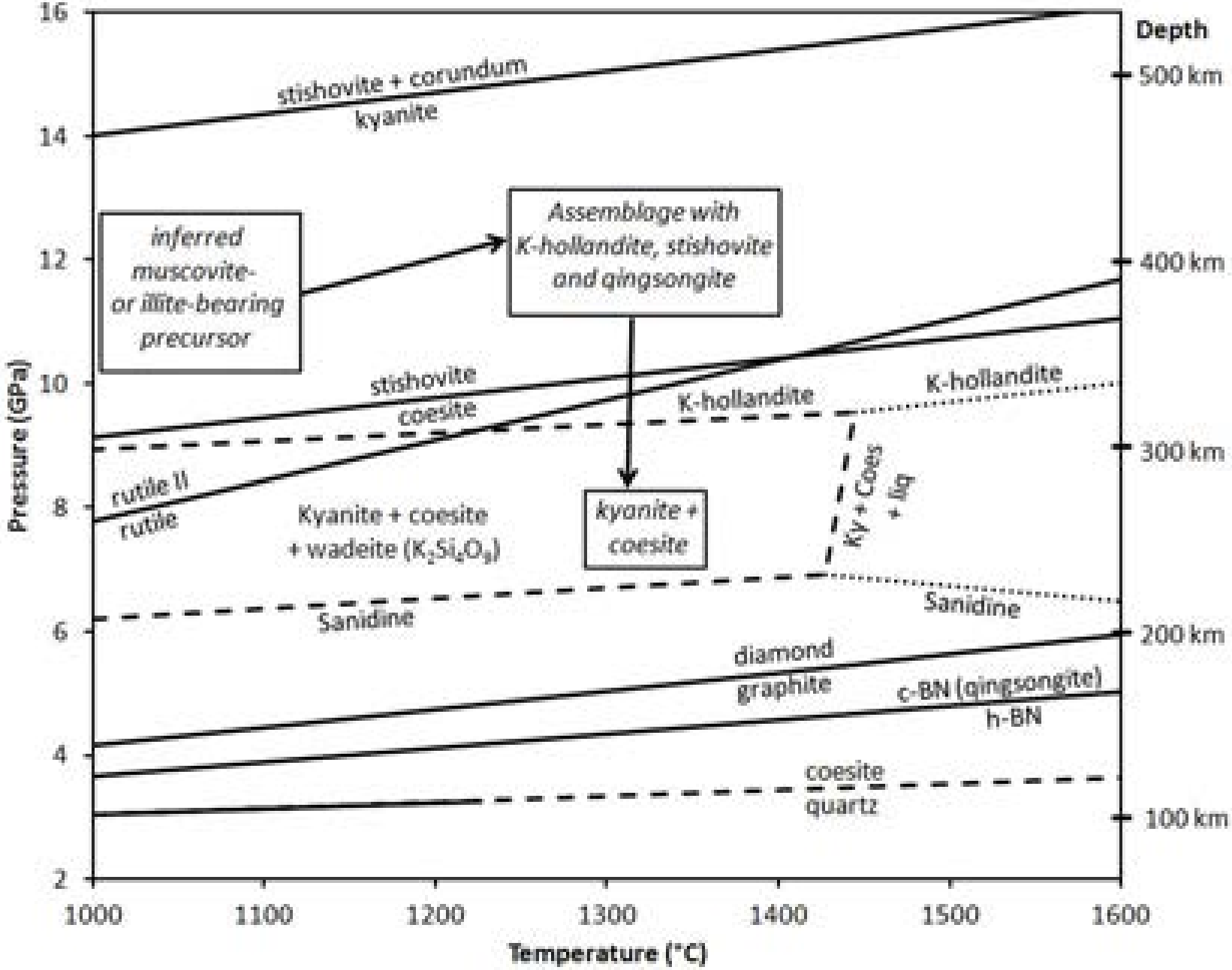
Depth
500 km
400 km
300 km
200 km
100 km
stishovite + corundum
kyanite
inferred muscovite- or illite-bearing precursor
Assemblage with K-hollandite, stishovite and qingsongite
stishovite
coesite
K-hollandite
K-hollandite
rutile II
rutile
Kyanite + coesite + wadeite ($K_2Si_4O_9$)
kyanite + coesite
Ky + Coes + liq
Sanidine
Sanidine
diamond
graphite
c-BN (qingsongite)
h-BN
coesite
quartz
Pressure (GPa)
Temperature (°C)
16
14
12
10
8
6
4
2
1000
1100
1200
1300
1400
1500
1600